RSC Advances

ROYAL SOCIETY OF CHEMISTRY

www.rsc.org/advances

TOC

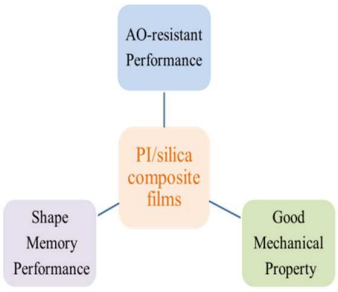

Shape memory polyimide/silica composite films show AO-resistant performance, good thermal stability and mechanical properties.

AO-resistant Shape Memory Polyimide/Silica Composites with Excellent Thermal Stability and Mechanical Properties

Zenghui Yang,[a,b] Qihua Wang,[a,*] Yongkang Bai[a,b] and Tingmei Wang[a]
[a] State Key Laboratory of Solid Lubrication, Lanzhou Institute of Chemical Physics, Chinese Academy of Sciences, Lanzhou, 730000, P. R. China.
[b] University of Chinese Academy of Sciences, Beijing, 100039, P. R. China
*Corresponding author: Qihua Wang (E-mail address: Wangqh@licp.cas.cn)

Abstract

Shape memory polyimide/silica (PI/silica) composites with atomic oxygen resistance, good thermal stability and mechanical properties are synthesized by co-condensation of poly (amic acid) terminated with (3-AminoPropy) triethoxysilane (APTES) and Tetraethoxysliane (TEOS) via sol-gel method. The silica networks formed in the hybrid films that not only as permanent crosslink point, but as atomic oxygen (AO) resistant moiety. The results show that the PI/silica composites films possess high thermal decomposition temperature (T_d>550 ℃), high glass transition temperature (T_g>265 ℃) as well as good shape fixation ratio (R_f>98%) and shape recovery ratio (R_r>90%). The mechanical properties, surface topography and shape memory performance of PI/silica composite films were evaluated before and after AO irradiation in simulated space environment. Compared to pristine PI, the mechanical properties, surface topography, and shape memory performances of PI-SiO_2-15 had less affected by AO exposure, which result from the silica protective layer formed on the composite films surface, indicating good AO-resistant ability of PI/silica composite films. This work may provide a strategy toward the design of promising shape memory materials for applications in the field of severe conditions.

Key words shape memory polymers, atomic oxygen, polyimide composites

Introduction

Shape memory polymers (SMPs), a kind of novel smart materials, have been rapidly developed during the past decades.[1-8] SMPs are capable of memorizing a temporary shape under a programming process and then recovering to their permanent (original) shape when exposed to suitable external stimulus such as light[9-11],

thermal[12,13], magnetic field[14], electric field[15], solvent[16-19]. Among all the form of SMPs, thermal-sensitive SMPs with low transition temperature have paid tremendous attention in both scientific and industrial applications, such as thermoplastic polyurethane elastomers (TPU), polynorbornene, polyvinyl alcohol (PVA), cross-linked polyethylene, cross-linked poly (ε-caprolactone), poly(ester amide), and epoxy composites etc.[20-24] These polymers with excellent shape memory performance, low transition temperature, and easily projected structure have enabled applications in biomedical materials,[25] smart textile,[26] self-healing,[27] active surface patterning,[28] and morphing structures.[29] However, these polymers have limited applications in some harsh environment, such as high temperature, high press, intense irradiation.

Aromatic polyimides (PIs) are widely used as engineering materials due to their excellent thermal stability, high glass transition temperature, superior mechanical properties and irradiating resistance capability.[30, 31] Recently, there are series of studies that focus on the shape memory performances of polyimides and their composites.[32-34] Our group elucidated the shape memory mechanism and the relationship between the structure and shape memory performance of PIs. Conclusion can be drawn that rigidity structure of polyimides have tight influence on shape memory effect, endowing PI based on ODA-BPDA structure has higher recovery ratio due to the stronger π-π interaction.[35]

Although PIs show high transition temperature, excellent mechanical properties as well as shape memory performances, the application is still a concern when the PI materials exposed to the harsh environments, for instance, the space environment in low earth orbit, where atomic oxygen (AO), UV irradiation, proton irradiation, space debris have a significant influence on polymers.[36-40] AO as one of the significant compositions in low earth orbit has major threat on polymers, leading to polymers loss its excellent performance and seriously reduce the service life of polymers and shorten the life time of the spacecraft.[41, 42] To the best of our knowledge, there are few reports about the influence of AO on SMPs. Therefore, it is highly valuable to develop shape memory polymers with high transition temperature, excellent mechanical properties as well as good shape memory performances.

In the present, we fabricated polyimide hybrid films with different load of silica by co-condensation of poly (amic acid) terminated by APTES and TEOS via sol-gel method. Introducing the cross-linked silica networks structure not only increase the shape memory performances due to the enhancement of hard phase by the cross-linked networks of silica, but strengthen the AO-resistant properties of polyimides. Moreover, the thermal, mechanical and shape memory properties of these PI/silica composite films were investigated before and after AO exposure, showing that the PI/silica composite films exhibit good thermal stability, excellent mechanical properties, good shape memory and AO-resistant performances. This work may provide a strategy toward the design of a promising shape memory material for applications in the field of severe conditions.

Experimental

Materials

4,4'-oxydianiline (ODA) was supplied by the Sinopharm Chemical Reagent Co., Ltd. 3,3',4,4'-Biphenyl Tetracarbolylic Acid Dianhydride (BPDA) was purchased from Shanghai Research Institute of Synthetic Resin. N-methyl-2-pyrrolidone (NMP) was obtained from Shanghai Kefeng industry & commerce Co., Ltd. (3-AminoPropyl) triethoxysilane (APTES, 99%) was received from Aladdin Reagent Co. Tetraethoxysliane (TEOS, 99%) was supplied by Alfa Aesar Chemical Reagent Co. All the reagents are used as received without further purify.

Synthesis of PI/silica composite films

In this study, the molar ratio of BPDA: ODA: APTES was 10: 9.9: 0.2 according to Carothers equation for step-grown polymerization.[43] Synthesis procedure via sol-gel method for PI/silica composite films were illustrated in scheme.1. Polyimide composite films were synthesized via three steps: synthesis poly (amic acid) terminated with APTES; co-condensation APTES and TEOS; cast films and thermal imidization. Taking polyimide/silica composite films (15 wt%) as an example. Briefly, ODA (9.9 mmol, 1.98 g) was added into a three-neck flask, then added NMP and kept stirring under nitrogen purge at room temperature. When the ODA completely dissolved, weighted BPDA (10 mmol, 2.94 g) slowly added into the flask. The mixture was stirred for 6 h at room temperature and then weighted APTES (0.2 mmol,

0.443 g) added into the solution and kept stirring another 6h. A viscous poly (amic acid) terminated by APTES with a solid content of 10% was obtained. TEOS (0.738 g), distilled H_2O (0.510 g) (molar ratio of TEOS:H_2O is 1:8) and HCl (as the catalyst) were subsequently introduced into the poly (amic acid) solution and stirred for 12 h at room temperature leading to completely hydrolysis. The obtained homogeneous and transparent poly (amic acid) solution was spread a cleaned glass pate and then imidized successively at 80 ℃ for 4 h, 100 ℃ for 1 h, 200 ℃ for 1 h, and 300 ℃ for 1 h. After, the glass pate immersed into hot water and the PI/silica composite films was peeled off from the glass substrate, the thickness was about 50 μm. Other PI/silica composite films were also synthesized use the same method.

Characterization

Fourier Transform Infrared (FT-IR) spectra were recorded at room temperature on Nexus 870 by the attenuated total reflectance (ATR) method. Thermal gravimetric analysis (TGA) was performed under nitrogen on a Netzsch-STA449F3 simultaneous thermal analysis system using a heating rate of 10 ℃ min^{-1} from 20 to 800 ℃. Dynamic mechanical thermal analyses of films were measured with a TA Instruments Netzsch DMA 242C heated from 25 ℃ to 400 ℃ at a rate of 5 ℃ min^{-1} and a frequency of 1 Hz. A universal testing machine (Shimadzu AG-X, 5000N) was used to study the mechanical properties with a constant crosshead rate of 5 mm min^{-1} at room temperature. The film samples were carefully cut to dog-bone type dimensions according to ISO527-2/1BB for tensile tests. The elemental components and valence variations of the polyimide composite films before and after AO exposure were analyzed by X-ray photoelectron spectra (XPS, ESCALAB 250X). The surface morphologies of composite films before and after AO exposure were observed via scanning electron microscope (SEM, JSM-6701F).

The AO irradiation on shape memory polyimide composites were carried out in a ground-based simulation facility in the Lanzhou Institute of Chemical Physics, Chinese Academy of Sciences. The average energy of the AO produced by this system was 5 eV and the flux of AO was determined to be 5.6×10^{15} atoms cm^{-2} s^{-1}. To discuss the effect of AO irradiation on the performances of shape memory polyimide

composite films, the pristine PI and PI-SiO_2-15 were selected to irradiate under AO for 1h, 3h, and 5h, respectively.

The shape memory properties of all samples were assessed by DMA. The shape fixation and recovery were quantitatively measured from shape memory cycles using a tensile film fixture and the controlled force mode of the DMA via the following process: the film sample was first heated to 350 ℃; a constant load was applied to stretch the sample when it equilibrated at 350 ℃; the sample was cooled under the constant load at a rate 5 ℃ min^{-1} to 20 ℃ in order to keep the temporary shape, then removed the constant load and hold for 5 min; reheated the sample up to 350 ℃ at 5 ℃ min^{-1} at free stress model and keep 1 h to completely achieve the shape recovery of the sample. All samples were repeated five shape memory cycles.

Results and discussion

The preparation of PI/silica composite films

The synthesis route of PI/silica composite films with different silica content was shown in scheme.1. In this study, the weight content of silica in composites is calculated from TEOS by assuming that the hydrolysis reaction proceeded completely. The samples are named as PI-SiO_2-X (X represents the SiO_2 content in composites). The incorporation of silica networks in polyimides were demonstrated by FT-IR measurement and SEM. The surface morphology of PI-SiO_2-15 seems smooth and the Si atom is uniform dispersed in the matrix (Figure.1a, b). The surface morphology of PI-SiO_2-15 etched with hydrofluoric acid indicated that the silica networks formed in the composites and had a good compatibility with organic polyimide phase (Figure.1c, d). FT-IR shows the characteristic absorption band of pristine PI and PI/silica composite films (Figure.S1). The appearance of characteristic bands at about 1770 cm^{-1} (C=O asymmetrical stretching), 1710 cm^{-1} (C=O symmetric stretching), and 1370 cm^{-1} (C–N stretching) are attributed to imide groups, which indicated that poly (amic acid) converted to the polyimide completely within the detection limit of IR. The absorption band appearance about 1100-1000 cm^{-1} (Si-O-Si symmetric stretching vibrations) and disappearance about 960 cm^{-1} (TEOS) confirmed that TEOS occurred hydrolysis and inorganic silica networks were successfully formed in polyimide

composite films by the sol-gel process.[44-46]

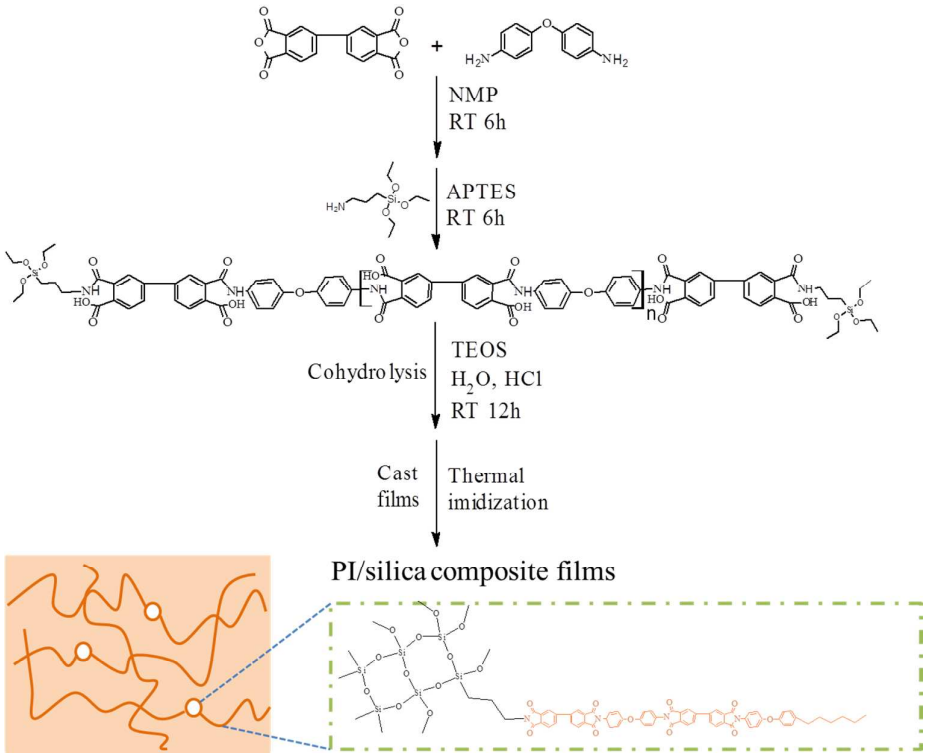

Scheme.1 Synthesis route of PI/silica composite films.

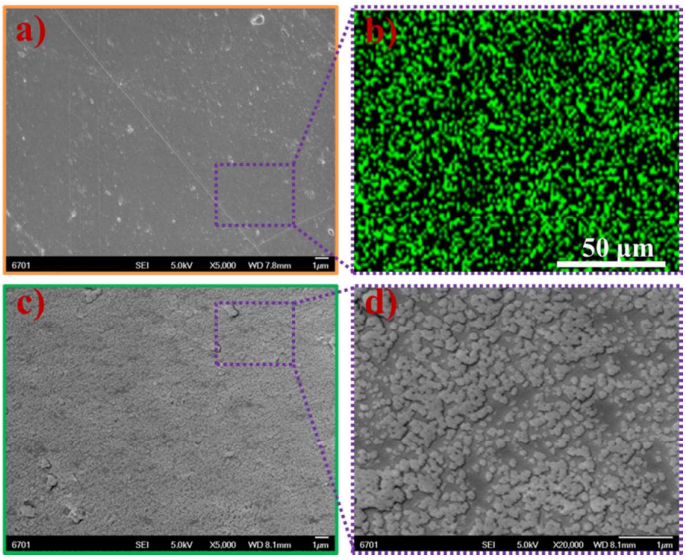

Figure.1 Surface morphology (a) and surface Si map (b) of PI-SiO_2-15; surface morphology of PI-SiO_2-15 after etching 24 h with HF (c) and the corresponding amplification image (d).

Thermal stability of prepared PI/silica composite films

The thermal decomposition temperature of PI and PI/silica composite films were

measured by TGA analysis. Figure.2 illustrates the TGA curves of the prepared PI/silica composite films. The onset decomposition temperature ($T_{d\text{-}onset}$) and the temperature of weight loss 10% ($T_{d\text{-}10\%}$) of the PI/silica composite films are summarized in Table.1. As indicated in Table.1, $T_{d\text{-}onset}$ and $T_{d\text{-}10\%}$ of the resulting films were above 550 ℃ and 570 ℃, respectively, showing that the PI/silica composite films have excellent thermal stability. The increase of the thermal stability is probably related to the higher thermal stability of silica and the strong interfacial interaction between polyimide matrix and inorganic silica. As indicated, the increasing residues at 800 ℃ from pristine PI to PI-SiO_2-15 also suggested the successful incorporation of the silica networks moiety in the hybrid polyimides. The residual ash from TGA analysis is lower than the calculated silicon content. The reason for this probably the unreacted TEOS volatilized during thermal imidization process. The mass loss of region between 200 ℃ and onset of clear change of TGA could be attributed to the volatilization of residual solvent and the imidization of few unreacted poly (amic acid) in imidization process.

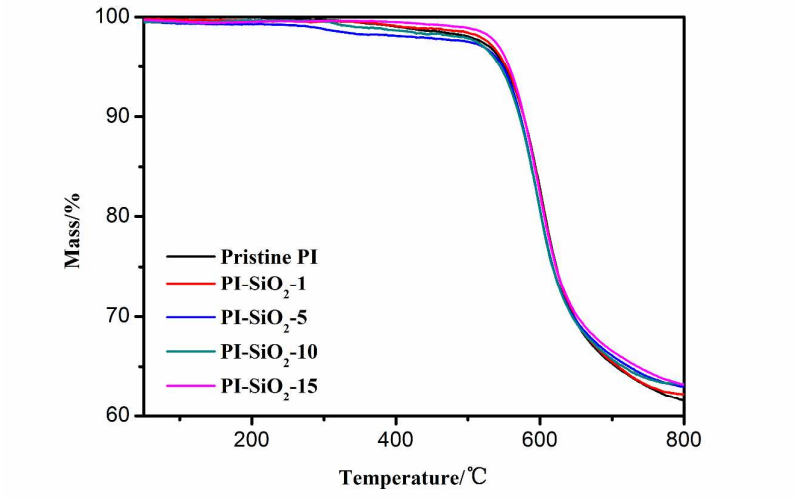

Figure.2 TGA curves for pristine PI and PI/silica composite films

Table.1 Summary of the thermal properties of PI and its composites

Sample code	T_g (℃)[a]	E'_{Tg-20} (MPa)	E'_{Tg+30} (MPa)	$T_{d-onset}$ (℃)[b]	$T_{d-10\%}$ (℃)[b]	Char yield (%)[c]
Pristine PI	264.2	1513.8±57.2	85.1±0.53	554.5	572.9	62.95
PI-SiO_2-1	274.5	1714.8±26.9	62.0±0.79	556.7	577.7	62.20
PI-SiO_2-5	272.5	1747.6±12.1	100.8±1.9	553.2	571.6	63.23
PI-SiO_2-10	282.3	1654.8±60.9	99.4±0.41	556.5	575.1	62.46
PI-SiO_2-15	283.5	1713.8±21.0	128.3±0.28	555.1	578.0	63.17

[a]T_g determined from the peak value in Tan δ curves using DMA
[b]Temperatures at begin to decompose and weight loss 10% were recorded using TGA
[c]Residual weight at 800 ℃ under nitrogen atmosphere

The linear viscoelastic properties of PI/silica composite films

The storage modulus (E') of SMP composite films, has a close relationship with shape memory effects, especially the E' in the rubbery state.[47] Figure.3 shows storage modulus (E') and loss factor (Tan δ) of PI and PI/silica composite films. Compared to pristine PI, the PI/silica composite films have enhanced storage modulus (E') both in the glass state at the low temperature and in the rubbery state at the high temperature with the increase the amount of inorganic phase silica (Table.1). The increase of E' ascribes to the cross-linked structure and the enhancement of silica in polyimide matrix because of the strong interfacial interaction between inorganic phase and organic phase. The E' at glass state maintains a high modulus plateau and at rubbery state keeps a lower modulus plateau under a wide range of high temperature (Figure.3a). Obviously, all of PI composite films show high ratio of storage modulus ratio in glass state to that in rubbery state, which are essential for excellent shape memory performance for shape memory polymers. Figure.3b shows the loss factor (Tan δ) curves as a function of temperature for PI/silica composite films. The temperature determined from the peak value in Tan δ represents the T_g. From Table.1, the pristine PI has a T_g of 264.2 ℃. It is seen that after introducing inorganic silica phase, the T_g of the composite films gradually increased, because cross-linked network formed through the covalent linkage between the organic phase and inorganic phase. Thus the organic PI molecular chain is restricted and higher temperature is needed to activate molecule chain segments motion.

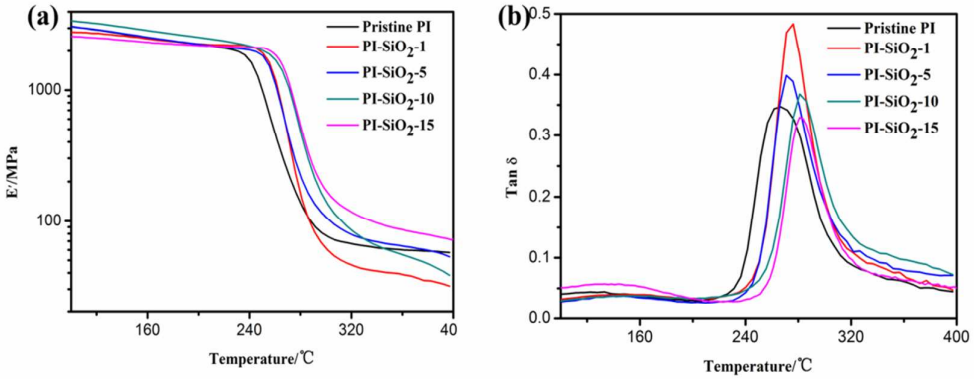

Figure.3 (a) Storage modulus and (b) loss factor of pristine PI and PI/SiO_2 composite films.

Mechanical properties of PI/silica composite films

Good mechanical property is a significant factor for polymer materials applied as structure devices. For PI/silica composite films, the typical stress-strain curves are shown in Figure.4a, b. It is obvious that the tensile strength increase from 109.7 MPa for pristine PI to 123.4 MPa for PI-SiO_2-1. The tensile strength of PI-SiO_2-5, PI-SiO_2-10, and PI-SiO_2-15 are 118.1 MPa, 120.8 MPa and 118.2 MPa, respectively. The breaking elongation decreased from 63.12% for pristine PI to 27.1% for PI-SiO_2-15 as the load of SiO_2 increase. These effects are mainly associated with the strong interfacial interaction between polyimide and silica due to forming cross-linked networks via co-hydrolysis APTES and TEOS. The strength and the toughness of the hybrid films, of course, are dependent upon the density of the crosslink. In an appropriate range of the crosslink density, the crosslinking could be beneficial for the strength. While, when the cross-linked degree keep constant, the free volume of internal molecular chain in composites increased with the increasing of SiO_2 content in polyimide composites, leading to weaker interaction of polyimide chain and brittleness for the polyimide composite films. In summary, the tensile strength and break elongation for all samples were above 105 MPa and 25%, respectively, which are good enough to apply polyimide composites as structure materials.[43] Nevertheless, we supposed that the AO erosion may have a great influence on polymers mechanical properties when the SMP materials service in the low earth orbit. To confirm the assumption, the mechanical properties of pristine PI and PI-SiO_2-15 upon AO

exposure were tested. The results are given in Figure.S2, Figure.S3, and Figure.4c, d. It's clearly seen that the mechanical performance tremendous changed after AO irradiation both on pristine PI and PI-SiO_2-15 composite films. Figure.3c shows that the tensile strength and break elongation of pristine PI decrease not obviously after 1 h AO exposure, yet reduce sharply when further exposed to AO. This may be related to the micro-crack generated on films surface under AO exposure (Figure.5), which induce the films easily break from crack during tensile. Meanwhile, for PI-SiO_2-15, the tensile strength increased slightly and the break elongation reduced sharply with the increasing of AO exposure time, which probably related to the silica protect layer formed during AO exposure. As aforementioned, all of PI/silica composite films exhibit the excellent thermal, mechanical properties, and viscoelastic properties.

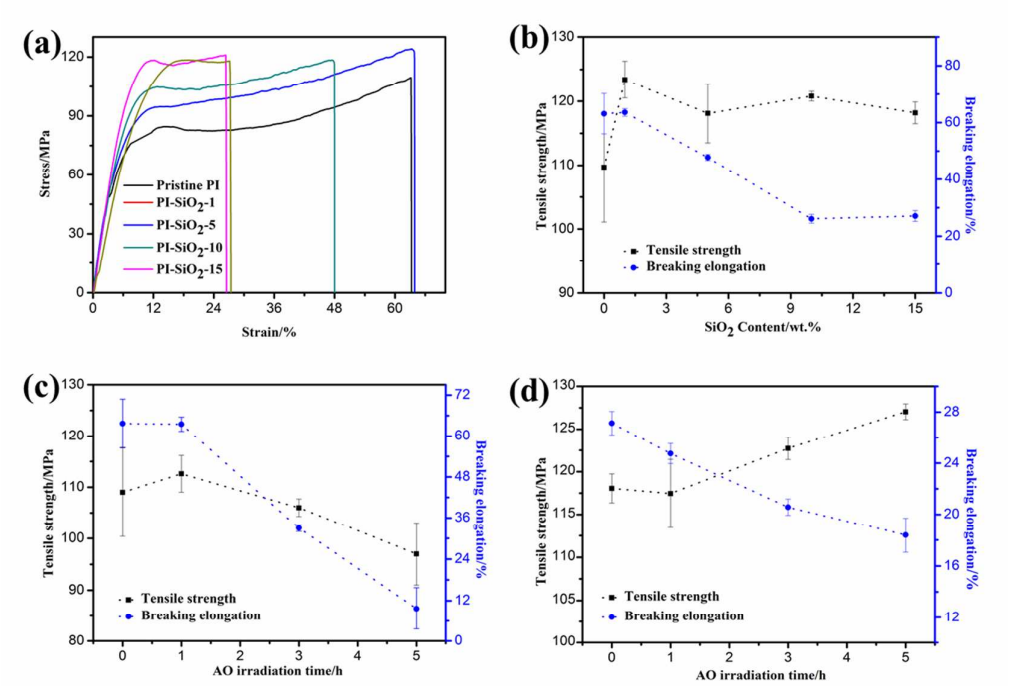

Figure.4 (a) Tensile stress-strain curves of pristine PI and PI/SiO_2 composite films, mechanical properties of (b) PI composite films with the increase of SiO_2 content, (c) pristine PI with the increase of AO exposure time, and (d) PI-SiO_2-15 with the increase of AO exposure time.

The surface morphologies of PI/silica composite films after AO exposure

The photos of SEM are presented in Figure.5 for the pristine PI and PI-SiO_2-15 films before and after AO exposure. Before AO irradiation, the films surfaces are smooth

and flat as shown in Figure.5a and e. While, the surface morphologies dramatically changed with increasing the AO exposure time, especially for the pristine PI film surface. Showing in Figure.5b-d, the pristine polyimide film surface became rough with the time of AO irradiation increase and exhibited a "carpet-like" morphology. One can draw conclusion that after 5h AO exposure, the "carpet-like" morphology broadened and deepened, even some deep ditches can be seen in the surface, as a results of the films transparency, mechanical properties, and surface roughness are affected. The PI-SiO_2-15 surface also became rough with the increase of AO exposure time, but the extent lower than the pristine PI. It is obvious that the hybrid PI surface have some region left after AO exposure. This was possibly because the AO reacted with surface atoms, thus the carbon, hydrogen, and nitrogen, all volatilized by the form of CO_2, CO, and H_2O. Meanwhile, the silicon are left in the surface forming silica with oxygen, and the silica-rich layer slowly formed which maybe as protective layer to prevent AO from further eroding composite films surface .[40]

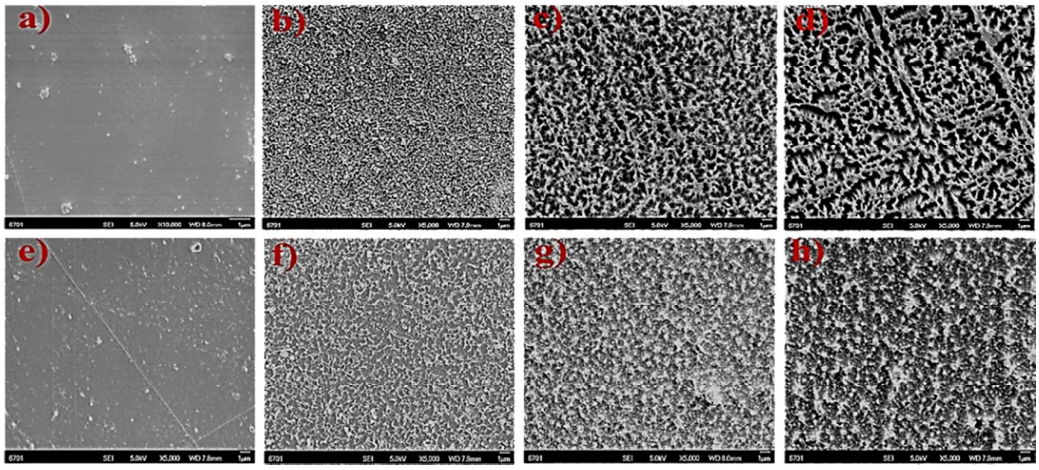

Figure.5 The influence of different AO irradiate time on the surface topography of pristine PI: (a) without irradiation, (b) 1h, (c) 3h, (d) 5h, and PI-SiO_2-15 films: (e) without irradiation, (f) 1h, (g) 3h, (h) 5h.

XPS analysis

To further prove the formation of silica on composite films surface, the oxidation state and surface compositions of pristine PI and PI-SiO_2-15 with different AO exposure time were analyzed by XPS. Table.2 and Figure.6 exhibit the changes of surface atoms content and valence states before and after AO exposure. For the pristine PI

surface, the carbon and nitrogen atoms content changed inconspicuously, and the oxygen atom slightly increased with the time increasing of AO exposure. While, for the PI-SiO_2-15 film surface, the carbon and nitrogen atoms content decreased significantly, meanwhile, the oxygen and Silicon atoms content increased obviously, indicating the silica layer formed.

Table.2 Surface atom concentrations (atom %) for pristine PI and PI-SiO_2-15 films before and after AO exposure to a variety time

Sample code	AO flux (5.6×10^{15} AO cm^{-2} s^{-1})	C 1s	N 1s	O 1s	Si 2p
Pristine PI	0h	76.26	3.73	20.01	0
	1h	69.56	4.27	26.17	0
	3h	71.02	4.06	24.92	0
	5h	68.95	4.93	26.12	0
PI-SiO_2-15	0h	63.13	4.05	21.98	10.84
	1h	57.80	4.94	27.44	9.82
	3h	46.07	3.30	36.32	14.31
	5h	41.08	2.88	40.52	15.52

High resolution XPS spectra C 1s, O 1s, and Si 2p peaks of PI-SiO_2-15 with variety time of AO exposure are shown in Figure.6. Obviously, the peaks at 248.6 eV (C-C or C-H) became slightly less pronounced after AO exposure and decreased sharply with the increase of AO exposure time. This is to say that the top surface atom concentration changed due to the oxidative degradation of organic polyimide moiety by AO. The Si 2p peak variation results of PI-SiO_2-15 before and after AO exposure to a variety of time are shown in Figure.6c. One can see, before AO exposure, mostly of silicon atoms existed in the form of Si-O-Si networks with a low binding energy about 102 eV. While, the surface silicon converted to silica after AO exposure with the binding energy formed about 103.5 eV, which are consistent with the results from SEM analysis. From the change of O1s binding energy (Figure.6b) also illustrated the surface organic polyimide degraded and the inorganic silica layer formed. We can infer that the surface retained silica will be total if films exposed to AO with more time. Therefore, inorganic silica was left on the surface of composite films after AO

exposure, which was not sensitive to AO and protected the underlying polymer from further degradation.[40] Here, we can conclude that the silica layer are formed on the composite film surface and has an influence on mechanical properties of hybrid polyimides.

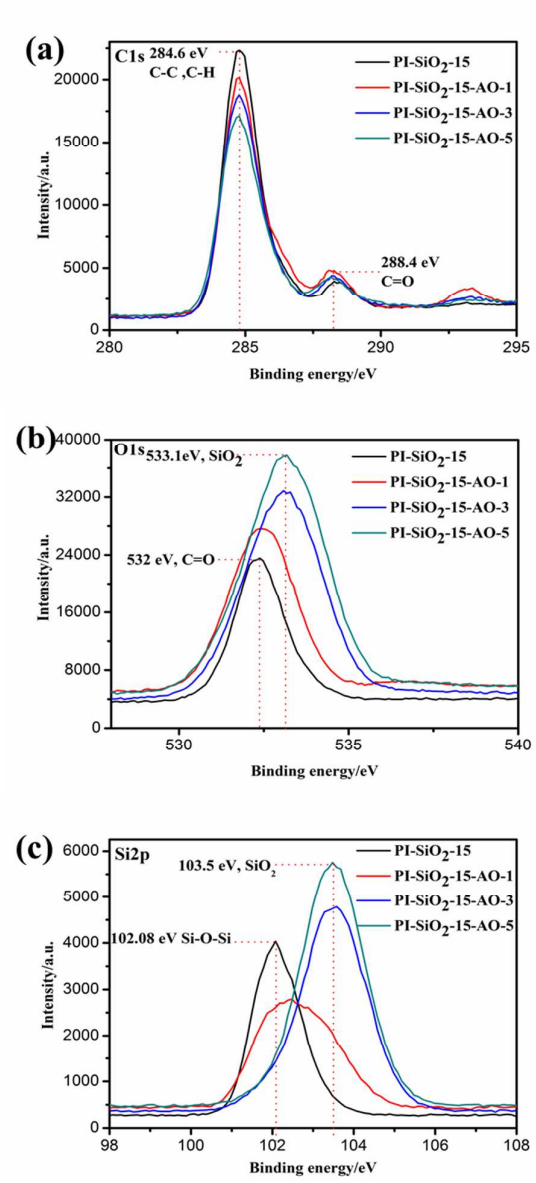

Figure.6 High-resolution XPS spectra of PI-SiO_2-15 polyimide films (a) C 1s, (b) O 1s and (C) Si 2p before and after AO exposure with AO exposed time of 1 h, 3 h, and 5 h.

Shape memory performances

The typical shape memory cycle sequences of polyimide composites are shown in Figure.7. The dots represent the crosslink networks of silica, which act as permanent

chemical crosslink point in shape memory behaviors, simultaneously, as AO-resistant moiety in materials. The entanglements of molecular chain act as physical crosslink point. The vitrification of polyimide chains act as the temporary crosslink point to fix the temporary shape. For SMPs, generally, the shape memory effects are evaluated by the thermo-mechanical cycle that contains a shape programming step and a recovery step. For shape programming step, the deformation is carried out at temperatures above the thermal transition temperature of the SMPs soft segment. The shape fixation of the temporary shape is achieved by cooling to temperatures below transition temperature while holding the deformation stress. For shape recovery step, the shape recovery to permanent shape will accomplish under free recovery condition when reheating the programmed SMP to switch temperature above the transition temperature. The sample will return to its original shape if the shape recovery ratio equal to 100%.

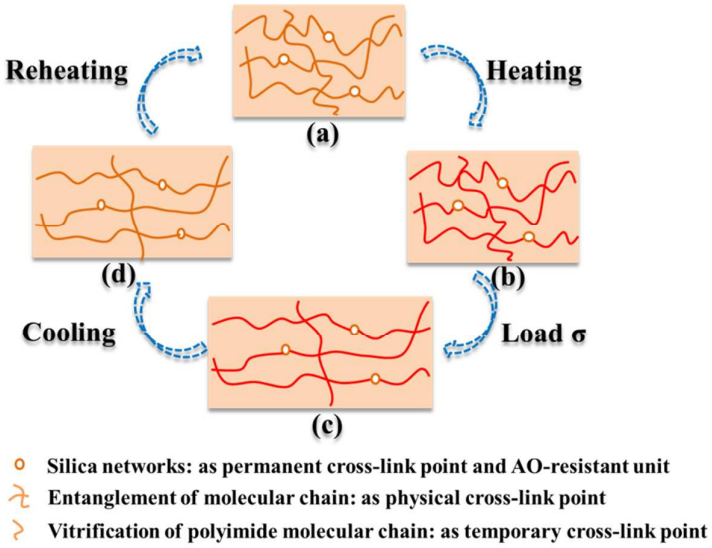

Figure.7 Schematic illustrates of shape memory behaviors

To quantitative evaluation the shape memory abilities, cycle thermo-mechanical measurements were performed on the DMA by the tensile mode. The representative shape memory cycle curves are shown in Figure.8 for pristine PI and PI-SiO_2-15. The shape memory properties are evaluated by shape fixation (R_f) and shape recovery ratio (R_r) according to equation (1) and (2). R_f represented the capability of fixing the

temporary shape, while R_r represented the capability of recovering to the original shape. Where ε_0 represents the initial shape and ε_{load} represents maximum strain under load, ε is the fixed strain after cooling to room temperature, and ε_{rec} is the strain after shape recovery.

$$R_f = (\varepsilon - \varepsilon_0)/(\varepsilon_{load} - \varepsilon_0) \quad (1)$$

$$R_r = (\varepsilon - \varepsilon_{rec})/(\varepsilon - \varepsilon_0) \quad (2)$$

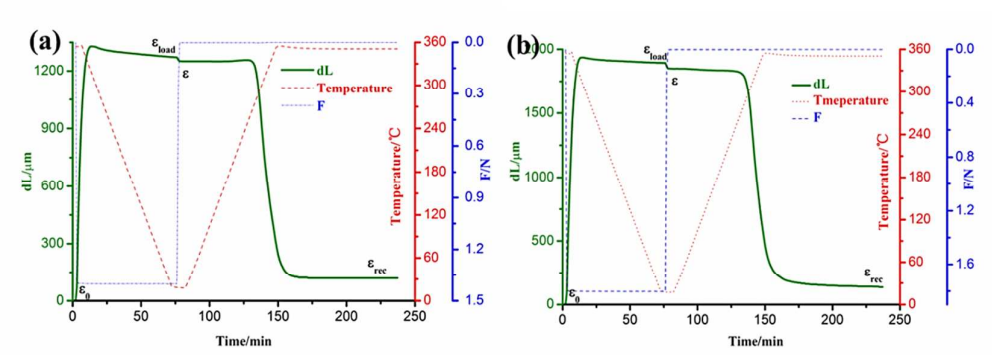

Figure.8 The representative shape memory cycles of (a) PI and (b) PI-SiO_2-15.

Figure.9 exhibits the shape fixation and recovery ratio curves verse cycle numbers, and details are summarized in Table.S1. One can see that all the composites show good shape fixation and shape recovery rate after five cycles. As observed from Figure.9, PI/silica composite films own higher shape recovery rate than pristine PI because of the higher E' in the rubbery state. From Lin and Chen's dashpot model for thermoplasticity SMPs, the shape fixation and shape recovery ratio are related to the ratio of storage modulus under low temperature to that above glass temperature.[48] For the PI composite films with higher storage modulus at high temperature, more deforming energy is needed at programmed temperature and more energy are stored with the loss of elastic entropy when cooling down to room temperature. As a result, the samples with higher storage modulus at high temperature have higher tendency to return to their original shape. Therefore, the shape recovery ratio increased in PI/silica composite films, which corresponding to Lin and Chen's model. Meanwhile, shape fixation rate of all composite films decreased slightly, yet shape recovery rate

increased tightly with the increasing of cycle times and reached relatively constant after a few cycles. This program is a training process in SMPs as evidenced by previous studies.[49]

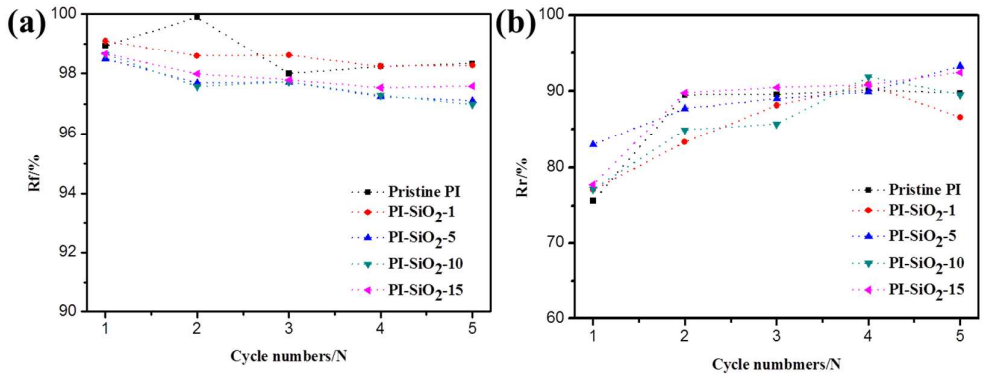

Figure.9 (a) R_f and (b) R_r verse cycle number curves of PI/silica composite films.

To explore the influence of AO on shape memory performance, we choose the pristine PI and PI-SiO_2-15 hybrid films to exposure to AO with 1h, 3h and 5h, respectively. The shape fixation and shape recovery ratio of composite films before and after AO irradiation were shown in Figure.10 and summarized in Table.S1. As indicted in Figure.10, the shape fixation ratio slightly decreased for both pristine PI and PI-SiO_2-15 after 5 h AO exposure. The shape recovery ratio for pristine PI increased at first and then decreased, yet the shape recovery ratio for PI-SiO_2-15 decreased slightly and reached nearly constant even further exposed to AO. These features are consistent with the change of mechanical properties and surface structure after AO exposure. The mechanical performance decreased and surface became roughness of pristine PI due to the breakage of surface segments after 1h AO exposure, yet this has no significant influence on shape memory effect. While, the shape fixation and shape recovery ratio of pristine PI all decreased dramatically when the films further exposed to AO environment. Hereto, we can predict that the shape memory performances of PI without AO resistant surface will reduce even loss when long-term exposed to AO environment.

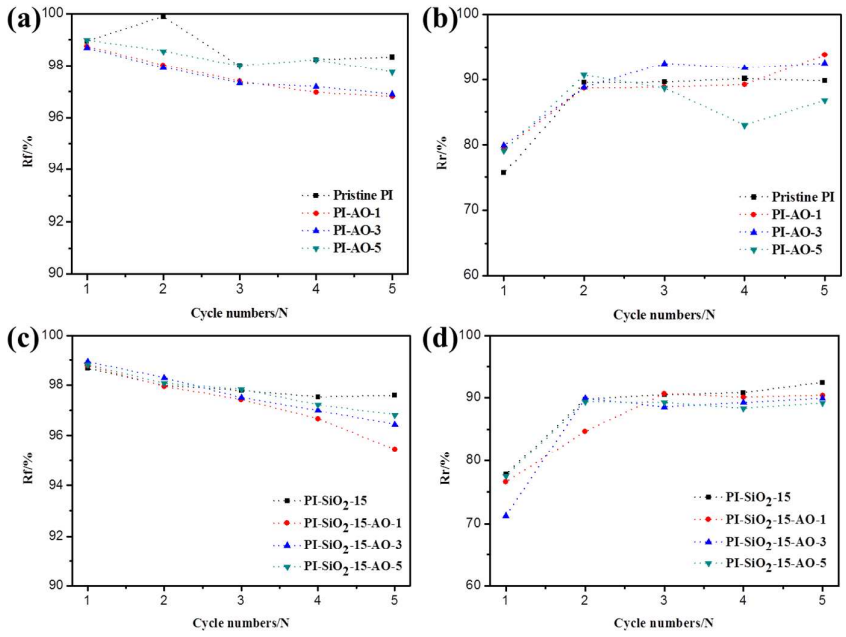

Figure.10 The influence of AO on R_f and R_r for pristine PI (a, b) and PI-SiO_2-15 (c, d) with different of AO exposure time.

Based on the above analysis from SEM and XPS results, the underlying polyimide of pristine PI were further degraded upon the longer time exposed to AO because there had no AO resistant layer, thus the surface sharply destroyed by the incoming AO, leading to the shape memory properties reduced. However, upon AO exposure, the on the topmost surface of PI/silica might be first eroded while silicon atoms left and gradually oxidized approximately to silica. It is the silica protective layer on the topmost surface of PI/silica composite films that have the ability of preventing AO from further eroding the underlying polyimide layer, as a result, the shape memory performances are changed inconspicuously. The protective mechanism can be illustrated visually as in Figure.11.

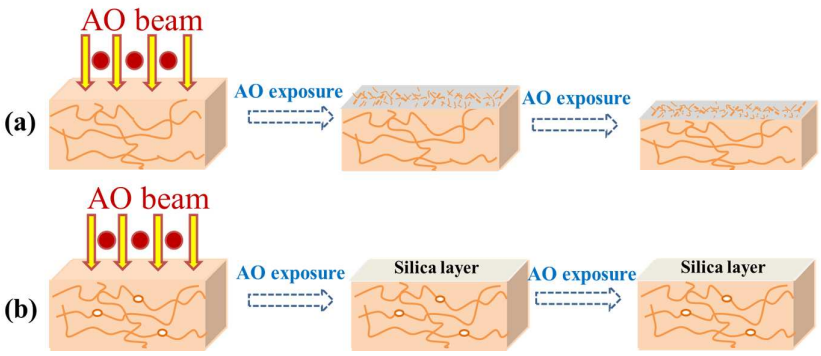

Figure.11 Schematic diagram of the erosion and protective mechanism of (a) pristine PI and (b) PI/silica composite films during AO exposure

Conclusions

In summary, we have fabricated Shape memory polyimide/silica composites films by co-condensation of poly (amic acid) terminated with APTES and TEOS via sol-gel method. The results show that the introduced inorganic silica phase has a good compatibility with organic polyimide, endowing the composite films superior thermal stability, atomic oxygen resistance, good mechanical properties as well as shape memory effects. In addition, the mechanical properties, surface topography and shape memory performances of the hybrid polyimides affected less by AO exposure than pristine PI. This could be ascribed to the protective effect by silica layer formed on the surface of PI/silica composite films during AO exposure. This study probably provides a direction of designing shape memory polymers to meet applications in harsh environment.

Acknowledgement

We greatly appreciate the financial supports from the National Basic Research Program of China (973 Program, Grant No. 2015CB057502), the National Defense Innovation Fund of Chinese Academy of Sciences (CXJJ-14-M43) and the National Natural Science Foundation of China (Grant 51305431) are duly acknowledged.

References

1. A. Lendlein and S. Kelch, *Angewandte Chemie International Edition*, 2002, **41**, 2034-2057.

2. M. Behl and A. Lendlein, *Materials Today*, 2007, **10**, 20-28.

3. J. Hu, Y. Zhu, H. Huang and J. Lu, *Progress in Polymer Science*, 2012, **37**, 1720-1763.

4. J. Leng and S. Du, *Shape-memory polymers and multifunctional composites*, CRC Press, 2010.

5. Q. Zhao, M. Behl and A. Lendlein, *Soft Matter*, 2013, **9**, 1744-1755.

6. G. J. Berg, M. K. McBride, C. Wang and C. N. Bowman, *Polymer*, 2014, **55**, 5849-5872.

7. M. Behl, M. Y. Razzaq and A. Lendlein, *Advanced materials*, 2010, **22**, 3388-3410.

8. Q. Meng and J. Hu, *Composites Part A: Applied Science and Manufacturing*, 2009, **40**, 1661-1672.

9. J. R. Kumpfer and S. J. Rowan, *Journal of the American Chemical Society*, 2011, **133**, 12866-12874.

10. A. Lendlein, H. Jiang, O. Junger and R. Langer, *Nature*, 2005, **434**, 879-882.

11. H. Zhang and Y. Zhao, *ACS applied materials & interfaces*, 2013, **5**, 13069-13075.

12. T. Xie, *Nature*, 2010, **464**, 267-270.

13. G. Rivero, L.-T. T. Nguyen, X. K. D. Hillewaere and F. E. Du Prez, *Macromolecules*, 2014, **47**, 2010-2018.

14. M. Y. Razzaq, M. Behl, K. Kratz and A. Lendlein, *Advanced materials*, 2013, **25**, 5730-5733.

15. J. Leng, W. Huang, X. Lan, Y. Liu and S. Du, *Applied Physics Letters*, 2008, **92**, 204101.

16. Y. Liu, Y. Li, H. Chen, G. Yang, X. Zheng and S. Zhou, *Carbohyd Polym*, 2014, **104**, 101-108.

17. K. Fan, *Express Polymer Letters*, 2011, **5**, 409-416.

18. H. Meng, J. Zheng, X. Wen, Z. Cai, J. Zhang and T. Chen, *Macromol Rapid Comm*, 2015, n/a-n/a.

19. H. Chen, Y. Li, Y. Liu, T. Gong, L. Wang and S. Zhou, *Polymer Chemistry*, 2014, **5**, 5168-5174.

20. H. Li, G. Sivasankarapillai and A. G. McDonald, *Industrial Crops and Products*, 2015, **67**, 143-154.

21. H. Li, G. Sivasankarapillai and A. G. McDonald, *J Appl Polym Sci*, 2015, **132**.

22. H. Li, G. Sivasankarapillai and A. G. McDonald, *J Appl Polym Sci*, 2014, **131**.

23. S. Mondal and J. Hu, *Journal of elastomers and plastics*, 2006, **38**, 261-271.

24. Q. Zhao, H. J. Qi and T. Xie, *Progress in Polymer Science*.

25. M. Behl, K. Kratz, U. Noechel, T. Sauter and A. Lendlein, *Proceedings of the National Academy of Sciences*, 2013, **110**, 12555-12559.

26. J. Hu, H. Meng, G. Li and S. I. Ibekwe, *Smart Materials and Structures*, 2012, **21**, 053001.

27. X. Luo and P. T. Mather, *ACS Macro Letters*, 2013, **2**, 152-156.

28. C.-M. Chen and S. Yang, *Advanced materials*, 2014, **26**, 1283-1288.

29. M. J. Higgins, W. Grosse, K. Wagner, P. J. Molino and G. G. Wallace, *The Journal of Physical Chemistry B*, 2011, **115**, 3371-3378.

30. T. St Clair, D. Yamaki and K. Mittal, *Plenum, New York*, 1984, **1**, 99.

31. M. Ghosh, *Polyimides: fundamentals and applications*, CRC Press, 1996.

32. J. A. Shumaker, A. J. W. McClung and J. W. Baur, *Polymer*, 2012, **53**, 4637-4642.

33. M. Yoonessi, Y. Shi, D. A. Scheiman, M. Lebron-Colon, D. M. Tigelaar, R. A. Weiss and M. A. Meador, *ACS Nano*, 2012, **6**, 7644-7655.

34. H. Koerner, R. J. Strong, M. L. Smith, D. H. Wang, L.-S. Tan, K. M. Lee, T. J. White and R. A. Vaia, *Polymer*, 2013, **54**, 391-402.

35. Q. Wang, Y. Bai, Y. Chen, J. Ju, F. Zheng and T. Wang, *Journal of Materials Chemistry A*, 2014.

36. X. Lei, P. Yao, M. Qiao, W. Sun, H. Zhang and Q. Zhang, *High Performance Polymers*, 2014, **26**, 712-724.

37. T. K. Minton, M. E. Wright, S. J. Tomczak, S. A. Marquez, L. Shen, A. L. Brunsvold, R. Cooper, J. Zhang, V. Vij, A. J. Guenthner and B. J. Petteys, *ACS applied materials & interfaces*, 2011, **4**, 492-502.

38. Z. Li, H. Song, M. He, J. Liu and S. Yang, *Progress in Organic Coatings*, 2012, **75**, 49-58.

39. K. Qi and G. Zhang, *Polym Composite*, 2014, n/a-n/a.

40. X. F. Lei, Y. Chen, H. P. Zhang, X. J. Li, P. Yao and Q. Y. Zhang, *ACS applied materials & interfaces*, 2013, **5**, 10207-10220.

41. H. Shimamura and T. Nakamura, *Polymer Degradation and Stability*, 2009, **94**, 1389-1396.

42. G. G. Odian and G. Odian, *Principles of polymerization*, Wiley-Interscience New York, 2004.

43. Y. Chen and J. O. Iroh, *Chemistry of Materials*, 1999, **11**, 1218-1222.

44. B.-K. Chen, T. M. Chiu and S.-Y. Tsay, *J Appl Polym Sci*, 2004, **94**, 382-393.

45. Z. Shang, C. Lü and L. Gao, *Polym Int*, 2006, **55**, 1277-1282.

46. J. Xu, W. Shi and W. Pang, *Polymer*, 2006, **47**, 457-465.

47. K. A. Watson, F. L. Palmieri and J. W. Connell, *Macromolecules*, 2002, **35**, 4968-4974.

48. J. R. Lin and L. W. Chen, *J Polym Res*, 1999, **6**, 35-40.

49. M. Heuchel, J. Cui, K. Kratz, H. Kosmella and A. Lendlein, *Polymer*, 2010, **51**, 6212-6218.